Translational Oncology 27 (2023) 101576

Contents lists available at ScienceDirect

Translational Oncology

journal homepage: www.elsevier.com/locate/tranon

Original Research

m6A demethylase FTO renders radioresistance of nasopharyngeal carcinoma via promoting OTUB1-mediated anti-ferroptosis

Wei-Mei Huang [a,1], Zhi-Xun Li [a,1], Ying-Hui Wu [b,1], Zhi-Ling Shi [a], Jing-Lin Mi [a], Kai Hu [a,*], Ren-Sheng Wang [a,*]

[a] Department of Radiation Oncology, First Affiliated Hospital of Guangxi Medical University, 6 Shuangyong Rd, Nanning, Guangxi 530021, China
[b] Department of Pathology, Sixth Affiliated Hospital of Guangxi Medical University, First People's Hospital of Yulin, Yulin 537099, China

ARTICLE INFO

Keywords:
Nasopharyngeal carcinoma (NPC), FTO,
Ferroptosis
m6A
OTUB1

ABSTRACT

Radiotherapy is a valid treatment for nasopharyngeal carcinoma (NPC), and radioresistance is the main cause of local NPC treatment failure. However, the underlying mechanisms and valuable markers of radioresistance for NPC remain have not been established. In this study, we observed that the m6A mRNA demethylase fat mass and obesity-associated protein (FTO) was significantly upregulated in radioresistant NPC tissues and cells relative to parental radiosensitive NPC tissues and cells. FTO enhances radioresistance by repressing radiation-induced ferroptosis in NPC. Mechanistically, FTO acts as an m6A demethylase to erase the m6A modification of the OTUB1 transcript and promote the expression of OTUB1, thereby inhibiting the ferroptosis of cells induced by radiation and finally triggering the radiotherapy resistance of NPC. Furthermore, our *in vivo* experiment results showed that the FTO inhibitor, FB23-2, and the ferroptosis activator, erastin, altered tumor responsiveness to radiotherapy in NPC cell lines and patient-derived xenografts. Our findings reveal, for the first time, that FTO enhances NPC radiotherapy resistance by withstanding radiation-induced ferroptosis, suggesting that FTO may serve as a potential therapeutic target and valuable prognostic biomarker in patients with NPC.

Introduction

Nasopharyngeal carcinoma (NPC) is a malignant tumor that occurs in the epithelium of the nasopharynx and is closely associated with Epstein-Barr virus (EBV), which is highly prevalent among people from southern China, Southeast Asia, and North Africa [1]. Since NPC typically arises in a relatively inaccessible location that is not amenable to surgery and is sensitive to ionizing radiation (IR), induction chemotherapy combined with concurrent chemoradiotherapy (CCRT) or CCRT alone is used as the routine and main treatment [2,3]. The 5-year overall survival rate of NPC patients has improved significantly (from approximately 17–35% to > 75%) with the development of radiotherapy technology in the past decades [4,5]; however, there is still a subset of 10–20% of patients with NPC who develop resistance to radiotherapy, which eventually leads to local recurrence and distant metastasis within 5 years [6]. Therefore, understanding the molecular mechanisms of residual NPC cells after radiotherapy is meaningful to overcoming the failure of NPC treatment.

In recent decades, m6A (N6-methyladenosine) has emerged as the most frequent modification of RNA and is considered the main regulator of intracellular gene expression [7]. Dysregulation of m6A frequently occurs in several pathological conditions, particularly in cancers, largely due to the aberrant expression of its related regulatory proteins [8]. Redressing RNA modification dysfunction by targeting m6A regulators is an attractive strategy for re-sensitizing cancer cells for radiotherapy [9]. Fat mass and obesity-associated protein (FTO) belongs to the Fe2+- and 2-oxoglutarate (2OG)-dependent AlkB dioxygenase family and is the first reported m6A demethylase in eukaryotes [10]. Recently, several studies have demonstrated that FTO plays oncogenic roles in various cancers, including leukemia, colorectal cancer, and breast cancer [11–13], which presents an opportunity for the development of effective FTO-targeted therapies for cancers. Su successfully developed two

Abbreviation: m6A, N6-methyladenosine; FTO, fat mass and obesity-associated protein; NPC, nasopharyngeal carcinoma; IR, ionizing radiation; ROS, reactive oxygen species; LPO, lipid peroxides; PDX, patient-derived xenografts; OTUB1, OTU deubiquitinase, ubiquitin aldehyde binding 1; HNSC, head-neck squamous cell carcinoma; OS, overall survival; RFS, recurrence-free survival; CCRT, concurrent chemoradiotherapy.

* Corresponding authors.
E-mail addresses: hukaigxmu@163.com (K. Hu), 13807806008@163.com (R.-S. Wang).
[1] These authors contributed equally to this work.

https://doi.org/10.1016/j.tranon.2022.101576
Received 26 August 2022; Received in revised form 6 October 2022; Accepted 18 October 2022

potent small-molecule inhibitors against FTO and found that FTO inhibition shows anti-tumor effects for several types of cancers in mouse models [11]. However, the role of FTO in NPC and its association with the radiotherapy resistance of the disease remain unclear.

Ferroptosis is a recently identified and regulated cell death process characterized by iron accumulation and lipid peroxidation [14]. Recent research has reported that ferroptosis is an important mechanism in radiotherapy-mediated tumor cell death and acquired radioresistance, although the exact genetic context of ferroptosis in cancer cells during radiotherapy is unclear [15].

In this study, by comparing the expression levels of FTO in radiotherapy-resistant and radiotherapy-sensitive NPC cells and tissues, we found that FTO is significantly highly expressed in radiotherapy-resistant NPC tissues or cells. Further *in vitro* and *in vivo* studies reported that FTO rendered NPC resistant to radiotherapy via enhancing OTUB1-mediated anti-ferroptosis. Meanwhile, we found that the ferroptosis inducer effectively promoted radiation-induced apoptosis of NPC cells. The relationship between FTO, OTUB1-dependent anti-ferroptosis, and radioresistance was investigated in this study.

Materials and methods

Tumor specimens and cell cultures

Fresh NPC tissues were obtained from the First Affiliated Hospital of Guangxi Medical University and approved by the appropriate ethics committee. Informed consent was obtained from all NPC patients before specimen collection. The two NPC cell lines (C666-1 and HONE1) used in this study were obtained from Shanghai Cell Bank, cultured in RPMI-1640 medium (Gibco, Hangzhou, China) supplemented with 10% fetal bovine serum (FBS; Gibco, New York, USA), and incubated at 37 °C in an atmosphere with 5% CO_2. Mycoplasma was administered once per month to eliminate contamination.

The two relatively radiation-resistant sublines C666-1R and HONE1R were established in our laboratory by irradiating C666-1 and HONE1 cells with a fractionated dose of X-rays (137Cs, Gammacell-40, Varian, Canada) of 4 Gy for 15 times (60 Gy in total) at a rate of 400 cGy/min. Cells were irradiated once per week. After fractionated irradiation at 60 Gy, the surviving cells, named C666-1R and HONE1R cells, were more radioresistant than the corresponding parent cells, which are C666-1 and HONE1.

Colony formation assay

The NPC cells were plated in a six-well plate at a uniform density of 200 cells/well. After 24 h, the cells were exposed to 4 Gy of X-rays. Seven to twelve days after irradiation, cell colonies were fixed with methanol and stained with 0.5% crystal violet.

Western blot assay

RIPA lysis buffer (CWBIO, Beijing, China) supplemented with a phosphatase inhibitor cocktail (CWBIO, Beijing, China) and protease inhibitor cocktail (CWBIO, Beijing, China) was used to extract the total cellular proteins. The protein concentrations were measured using a Bradford Protein Assay Kit (Beyotime Biotechnology, China) and denatured in SDS-PAGE loading buffer (Beyotime Biotechnology, China) at 100 °C for 5–10 min. Aliquots of protein (30–50 μg/sample) were separated by 8–12% SDS-PAGE, electrotransferred to PVDF membranes (Millipore, IPVH00010; Billerica, MA, USA), and blocked with 5% bovine serum albumin (BSA; MRC BIOTECH, Beijing, China) in Tris-buffered saline supplemented with 1% Tween-12 (TBST) for 1 h at room temperature. Finally, the PVDF membranes were incubated overnight at 4 °C with anti-FTO antibody (1:1000, Proteintech), anti-OTUB1 (1:2000, Abcam), SLC7A11 (1:1000, Proteintech), or anti-GAPDH (1:5000, CST), which was followed by a corresponding HRP-conjugated secondary IgG antibody for 1–2 h at room temperature. Chemiluminescent WB reagents (Millipore Corporation, Billerica, MA, USA) were used to detect the immunocomplexes, and GAPDH served as the loading control in this study.

RNA extraction and quantitative real-time PCR assay

RNAiso Plus* (Takara, Japan) was used to extract total RNA, according to the manufacturer's instructions. Total RNA concentration was measured using NanoDrop equipment. Reverse transcription of total RNA (500 ng) into cDNA was carried out in a 20 μl reaction system using a Fast Quant RT Kit (TIANGEN BIOTECH, Beijing, China). For the FTO transcript, the forward primer was 5'-AGA ATG TCT GTG ACG ATG TGG-3,' and the reverse primer was 5'-GCA CTT TCT GTA TCG ATT GCC-3'. For OTUB1, the forward primer was 5'-CCT TCA AAC GTG TGG GGT CT-3,' and the reverse primer was 5'-GCG GGG AAG AAA AGA GGT GA-3'. Finally, PCR was performed using a 2 × Talent qPCR PreMix (TIANGEN BIOTECH, Beijing, China). Human GAPDH (Sangon Biotech, China) was used as an internal reference in this study. Relative mRNA levels were analyzed using the $2^{-\Delta\Delta Ct}$ method.

Transient transfection

The Flag-FTO and corresponding control plasmids were purchased from GeneChem (Shanghai, China). The TIANprep Mini Plasmid Kit (TIANGEN, China) was used to purify the plasmid DNA. Transient transfection experiments were performed using the Lipofectamine 3000 reagent kit (Invitrogen) according to the manufacturer's instructions.

Drug treatment

FB23-2 (Selleck, China) is an inhibitor that directly binds to FTO and selectively inhibits the m6A demethylase activity of FTO in mammalian cells [16]. Ferrostatin-1 (fer-1, Selleck, China) is an effective and selective ferroptosis inhibitor, while erastin (Selleck, China) is a ferroptosis activator that acts on mitochondrial VDAC in cancer cells [17]. The three drugs were dissolved in dimethyl sulfoxide (DMSO) and stored at -80 °C. The NPC cells were treated with 10 μmol of FB23-2, 1 μmol of Fer-1, or 10 μmol of erastin in a medium containing 10% of FBS for 24–72 h, and the corresponding concentration of DMSO was used as a control.

Immunohistochemistry (IHC)

Clinical tumor tissues of NPC and xenograft mouse tissues embedded in paraffin were cut into serial 4μm thick sections and used for immunohistochemistry. Briefly, the specimens were deparaffinized in three changes of xylene and rehydrated by incubation in ethanol. The indirect streptavidin-peroxidase method was performed according to the manufacturer's instructions (MaxVision). Finally, images were acquired and analyzed.

Cell Counting Kit-8 (CCK-8) assay

NPC cells (500 cells/well) were seeded in 96 well plates and cultured in a 100 μL RPMI-1640 medium containing 10% FBS for 24 h. The cells were exposed to irradiation with the X-ray beam at 2, 4, 6, or 8 Gy and replaced with an RPMI-1640 medium containing different components and cultured for 24–72 h. Finally, the medium was replaced with 100 μl of RPMI-1640 medium containing 10% CCK8, and the absorbance was measured on a microplate reader (SYNERGY H1) at 450 nm.

Flow cytometry analysis

Cell apoptosis was analyzed using flow cytometry. After irradiation, the cells were harvested and washed with cold PBS. The cells were

incubated with annexin V-APC/FITC and PI/7-AAD (Beibo, China) for 15 min at room temperature. The intensity was measured using a FAC Scan (BD Biosciences, USA). Apoptotic cells were defined as annexin V-positive.

RNA immunoprecipitation (RIP) assay

RIP assays were performed using a Magna RIP™ RNA-Binding Protein Immunoprecipitation Kit (Millipore Corporation, Billerica, MA, USA), as previously described [18]. The NPC cells were harvested and lysed by using a lysis buffer. Five micrograms of m6A or FTO antibody, as well as normal rabbit lgG, was first incubated with magnetic beads to form a magnetic bead-antibody complex. The NPC cell lysates were then incubated with the magnetic bead-antibody complex overnight at 4 °C. Subsequently, RNA in the immunoprecipitates was purified according to the manufacturer's protocol. Finally, the extracted RNA was analyzed using qRT-PCR.

Cellular lipid measurement

The cells (2×10^5) were seeded into dishes and cultured for 24 h and treated with FB23-2 (10 μmol) or transfected with Flag-FTO. After 24 h, the cells were irradiated with X-ray beam at 4 Gy and were cultured again for 72 h. C11-BODIPY 581/591 (Thermo Fisher Scientific, D3861) was used to stain the NPC cells for 1 h at 37 °C and digested by trypsinization. The cells were rinsed and resuspended in PBS. Flow cytometry (Beckman Coulter Cytoflex LX) with 488 or 561 nm lasers was used for further analysis, and data were collected and analyzed using Flow Jo 10.0 (Ashland, Oregon-based FlowJo LLC).

Intercellular GSH and MDA assays

NPC cells were treated with FB23-2 (10 μmol) or transfected with Flag-FTO. After 24 h of being cultured, the cells were exposed to 4 Gy X-rays and were cultured again for 72 h. The cells were then rinsed with PBS, and the intracellular GSH or MDA levels were measured using the GSH Assay kit (Beyotime, S0053) and MDA Assay kit (Beyotime, S0131S).

Co-Immunoprecipitation

The NPC cells were first washed with cold PBS three times and lysed with cold lysis buffer (#A10022, Abmart, China) containing a protease inhibitor (Beyotime, China). They were further lysed using ultrasound and centrifuged at 14,000 g for 10 min, and the pellets were removed. Of the total cell lysate, 2.5% was taken as input, and the rest of the cell lysate was incubated with OTUB1 antibody and agarose beads overnight at 4 °C. After washing four times with 1 × washing buffer, the precipitated proteins were analyzed using immunoblotting.

N6-methyladenosine (m6A) RNA methylation detection

The m6A RNA methylation status of NPC cells was evaluated using an EpiQuik™ m6A RNA Methylation Quantification Kit (Fluorometric) according to the manufacturer's instructions. Briefly, total RNA was extracted from NPC cells and added to assay wells. The RNA-bound wells were rinsed with diluted washing buffer and incubated with the capture antibody. The wells were washed with washing buffer and incubated with the detection antibody, as well as an enhancer solution. Finally, the fluoro developer solution was added, fluorescence was measured, and the m6A RNA methylation status was determined.

NPC cell line-derived tumor xenograft model

Research involving animals was performed in compliance with the policies of the animal ethics committee of the Guangxi Medical University of China. Three- to four-week-old female BALB/c nude mice were obtained from Guangxi Medical University Laboratory Animal Center and maintained under SPF housing. NPC cells were resuspended in 100 μl of PBS and injected subcutaneously into the flanks of the nude mice. Mice were randomized to experimental groups 28 days after implantation and were injected intraperitoneally with the same volume of FB23-2 (2 mg/kg) or erastin (10 mg/kg) or vehicle every three days during radiation (4 Gy, once a week). The endpoint of all experiments was tumor size.

Establishment of the PDX model

PDX models using samples derived from patients have been described previously [18]. To establish a PDX model (P0), we cut the NPC tumor samples into 3–4 mm pieces and subcutaneously transplanted them within 4 h after surgical removal into 3–5 severely immunodeficient B-NDG® mice (BIOCYTOGEN, Beijing, China). Mice were euthanized when tumors reached 500 mm^3, and the tumors were removed. Subsequently, scalpel-dissected xenograft fragments were either immediately implanted into new NDG® mice for passaging or fixed in 4% paraformaldehyde (YongJin Biotech, Guangzhou, China) for pathological analysis.

Radiosensitivity testing of the PDX model

When the subcutaneous tumors of the PDX model reached 500 mm^3, the mice were randomized into erastin (10 mg/kg) treatment and vehicle control groups. Erastin and vehicle (1% DMSO+99% normal saline) were injected intraperitoneally as described above. The endpoint of all experiments was tumor size.

Transmission electron microscopy (TEM)

NPC cells were collected and fixed in an electron fixation solution (Servicebio). After the post-fixation with 1% osmium tetroxide and dehydration, the samples were embedded in Epon. The sample sections were then stained with uranyl acetate and examined on a transmission electron microscope (Tokyo, Japan).

Comet assay

Comet assay was performed according to the manufacturer's instructions (OxiSelect™ Comet Assay Kit). Briefly, NPC cells were first washed with cold PBS and then were mixed with agarose at 43 °C, spread on pre-coated slides with agarose and solidified at 4 °C. The slides were placed in an ice-cold lysis solution in the dark for 1 h at 4 °C and placed in an alkaline electrophoresis solution for 40 min. Electrophoresis was performed under alkaline conditions for 20 min at 25 V/cm at 4 °C. The slides were washed with neutralizing buffer and stained with DAPI. Comet images were obtained using a fluorescence microscope (Nikon).

Statistical analysis

All statistical tests were two-sided. Data are presented as means. Bar plots with error bars represent the standard error of the mean (SEM). All analyses were performed using Prism version 8.0. Throughout the article, * represents $p < 0.05$, ** represents $p < 0.01$, and *** represents $p < 0.001$.

Results

High FTO levels are closely associated with the radioresistance of NPC

Through analyzing the correlation between FTO expression and survival duration of patients with head-neck squamous cell carcinoma

(HNSC) based on the Kaplan–Meier plotter database (kmplot.com/analysis), we found that patients with higher FTO expressions had significantly shorter overall survival (OS) (Fig. 1A). For NPC as a member of HNSC, we tried to investigate the potential role of FTO in NPC. We first analyzed the levels of FTO mRNA and protein in three NPC tissues before and after radiotherapy. The results showed that both transcription and translation levels of FTO were overexpressed in post-radiotherapy NPC tissues (Fig. 1B, C). We speculated that the high expression of FTO was an important prognostic marker of NPC radioresistance because the elevation of FTO had been previously reported to be a risk factor for poor prognosis in several neoplasms, such as gastric cancer [19], breast cancer, and lung cancer [20].

To explore the contribution of FTO to the radioresistance of NPC, we first generated two relatively radioresistant cell lines by irradiating C666-1 and HONE1 cells with fractionated radioactive doses of up to 60 Gy in total, which we named C666-1R and HONE1R. The radioresistance of C666-1R and HONE1R cells was confirmed by CCK8, flow cytometry, and clone formation assays (Fig. 1D–F). The differential expression of FTO was then measured between radioresistant cells and their parents. Consistently, we found that the expression levels of FTO mRNA and protein were also significantly upregulated in the radioresistant cell lines (C666-1R and HONE1R) compared with those in the relatively radiosensitive cell lines (C666-1 and HONE1) (Fig. 1G).

FTO promotes the radiation resistance of NPC in vitro

We further demonstrated that FTO plays an essential role in the radioresistance of NPC. The activity of FTO in C666-1R and HONE1R cells was inhibited by the FTO inhibitor, FB23-2. It was found that cells treated with FB23-2 significantly sensitized NPC cells to irradiation (Fig. 2A–C). These confirmed the importance of FTO activity for radiotherapy resistance of NPC. Subsequently, C666-1 and HONE1 cells were overexpressed FTO (Fig. 2D). FTO-overexpressing NPC cells showed significantly increased survival compared to the control cells when exposed to radiation (0–8 Gy) (Fig. 2E–G). In addition, we observed milder DNA damage in C666-1 cells upon FTO overexpression and irradiation, while more severe DNA damage was observed in C666-1R cells upon irradiation when treated with the FTO inhibitor FB23-2 (Fig. 2H). These results indicated that high FTO expression increases radiation resistance in NPC cells.

FB23-2 suppresses NPC radiotherapy resistance in vivo

We further assessed the therapeutic effects of FB23-2 *in vivo* using a xenografted NPC model. BALB/C-nu/nu mice were xeno-transplanted with HONE1R cells, and four weeks of post-xeno-transplantation. FB23-2 (2 mg/kg) or its vehicle (DMSO) control was intraperitoneally injected into the individual mice once every three days until the endpoint. Simultaneously, transplanted tumors were locally exposed to 4Gy of X-ray irradiation five times (20 Gy in total) (Fig. 3A). Notably, FB23-2 injection substantially delayed the growth of HONE1 xenografts following radiation exposure (Fig. 3B, C, $p < 0.05$), suggesting that co-targeting FTO can efficiently sensitize tumors to iron radiation. Moreover, histochemical analysis of the NPC tumors by pH2A.X staining confirmed a severe DNA damage in the FB23-2 treatment tumors after radiation, and cell proliferation potential was worse in the FB23-2 treatment tumors as determined by Ki67 staining (Fig. 3D). These results indicate that the inhibition of FTO activity by FB23-2 re-sensitizes HONE1R xenografts to iron radiation.

Induction of ferroptosis contributes to the radiosensitivity of NPC cells

The intrinsic biological mechanism of radioresistance is becoming attractive when the regulatory role of FTO in radiation resistance is explicit. We first analyzed the expression profile changes upon FTO knockdown in HEK293T cells [21]. Interestingly, among the deregulated pathways, the genes involved in the regulation of lipoproteins, lipid transport, palmitate, and monooxygenase, which are hallmarks of ferroptosis, were found to be significantly enriched (Fig. 4A). Notably, ferroptosis is known as an important pathway in radiation-mediated tumor cell death [22]. We investigated the effect of radiation on ferroptosis in NPC cells. We used the C11-BODIPY probe, lipid peroxidation sensor, and MDA kit to detect the level of lipid peroxidation (lipid ROS) in NPC cells after radiation. The results showed that the lipid peroxidation product content in NPC cells increased significantly after irradiation (Fig. 4B, C). Consistent with these observations, the intracellular GSH levels decreased upon irradiation in NPC cells (Fig. 4D). The results of transmission electron microscopy also showed that NPC cells exhibited morphological characteristics of ferroptosis after radiation treatment; these are mitochondrial atrophy and mitochondrial ridge reduction (Fig. 4E). We further evaluated the effect of the ferroptosis inducer, erastin, on the radiosensitivity of NPC cells. The results showed that the concurrent use of erastin significantly enhanced the radiosensitivity of C666-1R cells, which was characterized by increased apoptosis after radiation (Fig. 4F).

These results demonstrate that ferroptosis is an important mechanism of radiation-induced cell death in NPC, and FTO might be a regulator of ferroptosis.

FTO promote radiotherapy resistance by antagonizing radiation-induced ferroptosis in NPC cells

As shown in Fig. 4A, gene functional analysis revealed that FTO was strongly associated with ferroptosis-associated signaling pathways. Next, we determined whether ferroptosis plays a role in FTO-mediated radiation resistance. The content of lipid peroxidation products increased when NPC cells (C666-1R, and HONE1R) were treated with the FTO inhibitor FB23-2 but decreased with the overexpression of FTO in the C666-1 and HONE1 cells (Fig. 5A, B). In addition, the intracellular GSH levels were lower in FB23-2 treated cells but increased in FTO-overexpressing cells compared with negative control cells in NPC (Fig. 5C). Similarly, it was found that the mitochondria shrank significantly upon inhibiting the activity of FTO by FB23-2, whereas the overexpression of FTO showed the opposite results (Fig. 5D), indicating that FTO plays an important role in inhibiting radiation-induced ferroptosis in NPC cells.

To assess whether FTO promotes radiotherapy resistance in NPC cells by inhibiting radiation-induced ferroptosis, we treated NPC cells with the ferroptosis inhibitor, ferrostatin-1(Fer-1), combined with FTO activity inhibition and evaluated the changes in cell sensitivity to radiation. The treatment with Fer-1 rescued FB23-2 stimuli-induced cell death and cell growth inhibition in the context of radiation, as confirmed by CCK8 and colony formation assays (Fig. 5E, F).

Together, these data indicate that high expression of FTO in NPC cells can inhibit the accumulation of lipid peroxide, and FTO may promote radiotherapy resistance in NPC by inhibiting radiation-induced ferroptosis.

FTO suppresses radiation-induced ferroptosis in an OTUB1 and SLC7A11-dependent manner

We measured the m6A changes on RNA in different NPC cells. However, our results were inconsistent with the findings of a previous study [16]. Although the demethylase FTO was highly expressed in radiation-resistant cells, we observed that the level of m6A in the radiation-resistant cells was significantly higher than that in the radiation-sensitive cell lines. We also found that the level of m6A decreased when the activity of the FTO enzyme was inhibited, while increased after FTO overexpression in NPC cells (Fig. 6A). These results indicate that FTO promotes, rather than reduces, the global level of m6A modification in NPC cells.

We continued to explore the regulatory effect of FTO on the m6A

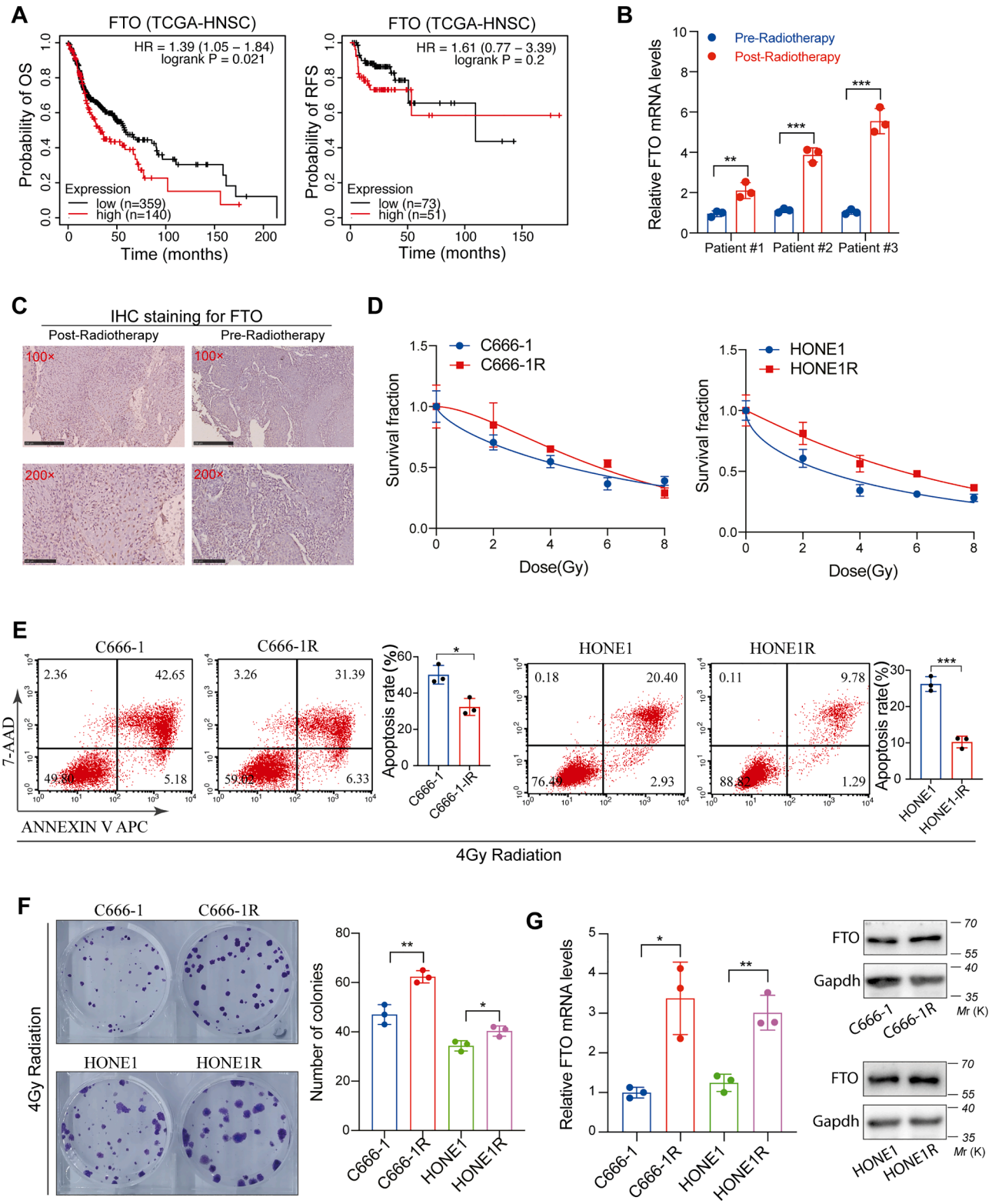

Fig. 1. High FTO levels are closely associated with the radioresistance of NPC. (A) Kaplan–Meier survival curves show the correlations between FTO expression and overall survival (OS, $p = 0.021$), as well as recurrence-free survival (RFS, no significance), in HNSC patients. (B-C) RT-qPCR assay and IHC staining were used to detect the level of FTO mRNA (Mean ± SEM, $n = 3$, two-sided t test) and protein in NPC tissues. (D) The CCK8 assay was used to detect the proliferation activity of indicated NPC cells after radiation (single-hit multitarget model was used to compare the sensitivity of different groups of cells to radiation). (E) Flow cytometry assay was used to detect the cell apoptosis after receiving 4 Gy radiation (mean± SEM, $n = 3$, two-sided t test). (F) Colony formation assay was used to test the proliferation activity of indicated cells after 4Gy radiation (mean ± SEM, $n = 3$, two-sided t test). (G) The mRNA and protein levels of FTO in indicated cells were detected by RT-qPCR assay and western blot assay (mean ± SEM, $n = 3$, two-sided t test).

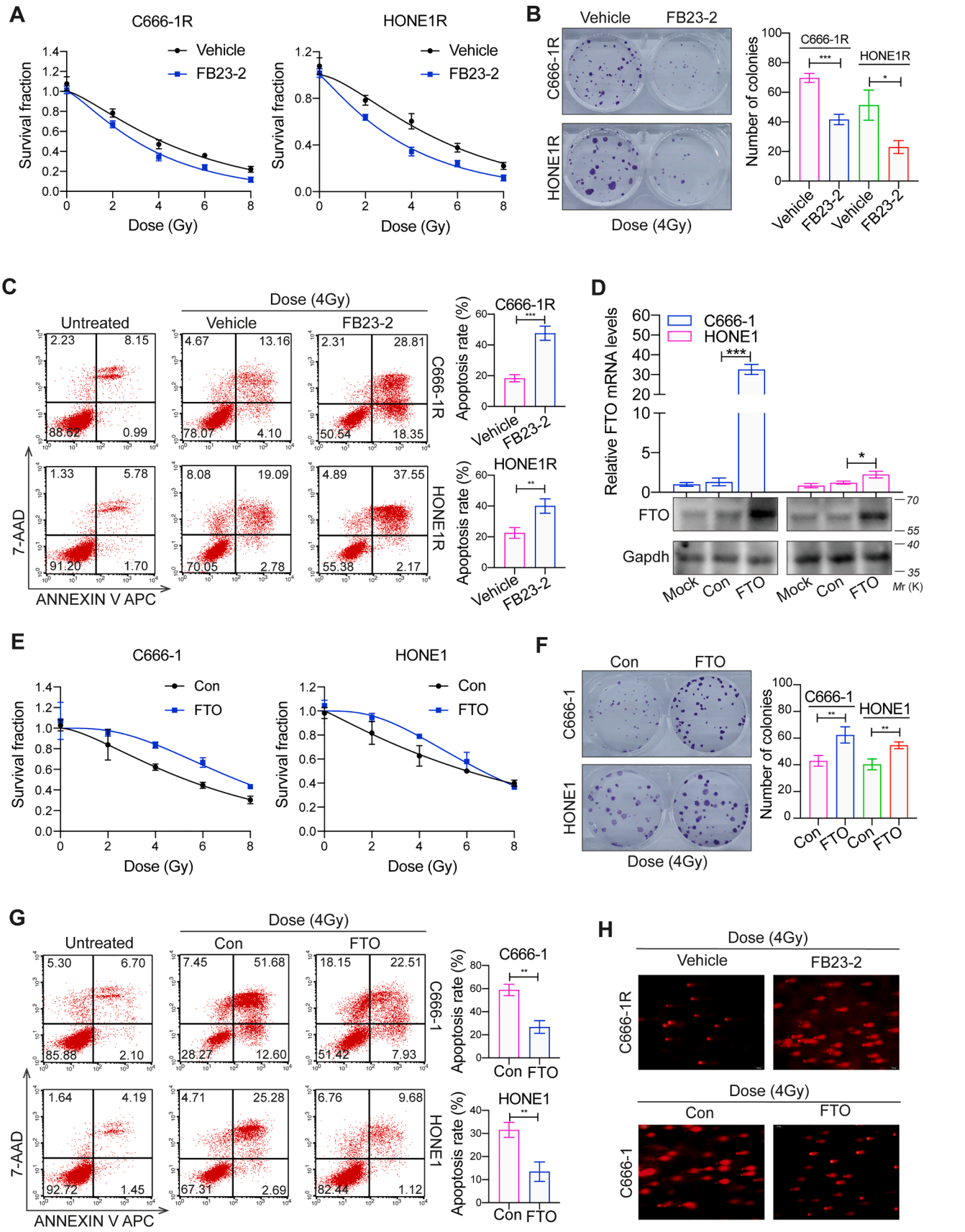

(caption on next page)

Fig. 2. FTO promotes the radiation resistance of NPC cells. (A) Dose responses of survival factions of C666-1R and HONE1R cells treated with or without FB23-2. (B) The proliferation of NPC cell lines was evaluated by colony formation assay under treatment with or without FB23-2 (mean ± SEM, $n = 3$, two-sided t test). (C) Treatment with an FTO inhibitor FB23-2 promoted the apoptosis of NPC cells after irradiation, confirmed by flow cytometry (mean ± SEM, $n = 3$, two-sided t test). (D) RT-qPCR assay and western blot assay were used to detect the expression of FTO and Gapdh in C666-1 and HONE1 cells after transfecting with Flag-FTO plasmid (FTO) or corresponding empty plasmid (Con). (E) Dose responses of surviving factions of C666-1 and HONE1 cells with or without overexpressing FTO. (F) Overexpression of FTO promotes the proliferation of NPC cells under radiation (4 Gy), which was confirmed by colony formation assay (mean ± SEM, $n = 3$, two-sided t test). (G) Overexpression of FTO inhibited the apoptosis of NPC cells under radiation (4 Gy), which was confirmed by flow cytometry assay (mean ± SEM, $n = 3$, two-sided t test). (H) Comet assay was used to evaluate the DNA damage of indicated cells after radiation (4 Gy).

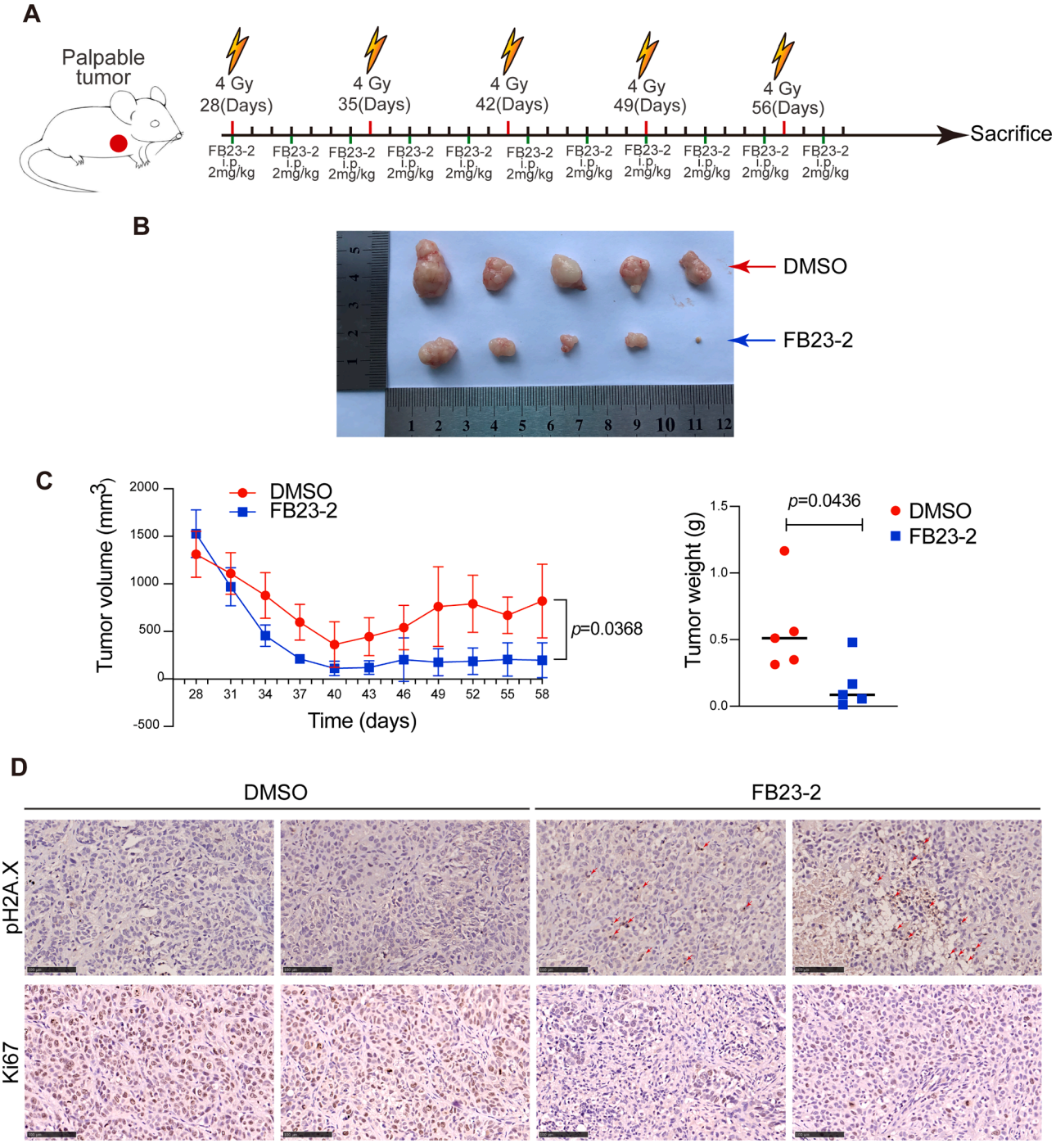

Fig. 3. FB23-2 suppresses NPC radiotherapy resistance *in vivo*. (A) Outline of the experimental approach. (B) Images of subcutaneous tumors comprising HONE1R cells after treating with FB23-2 or DMSO (Vehicle) ($n = 5$). (C) (Left) The growth curves of subcutaneous tumors derived from HONE1 cells with or without FB23-2 combination with radiotherapy are shown. (Right) Tumor weight (means, $n = 5$, two-sided t test) was measured at the endpoint. (D) Representative images of immunohistochemical staining of pH2A.X and Ki67 in tissue sections taken from tumors of the mice treated as indicated in (B). pH2A.X is a marker of DNA damage. Scale bars, 100 μm.

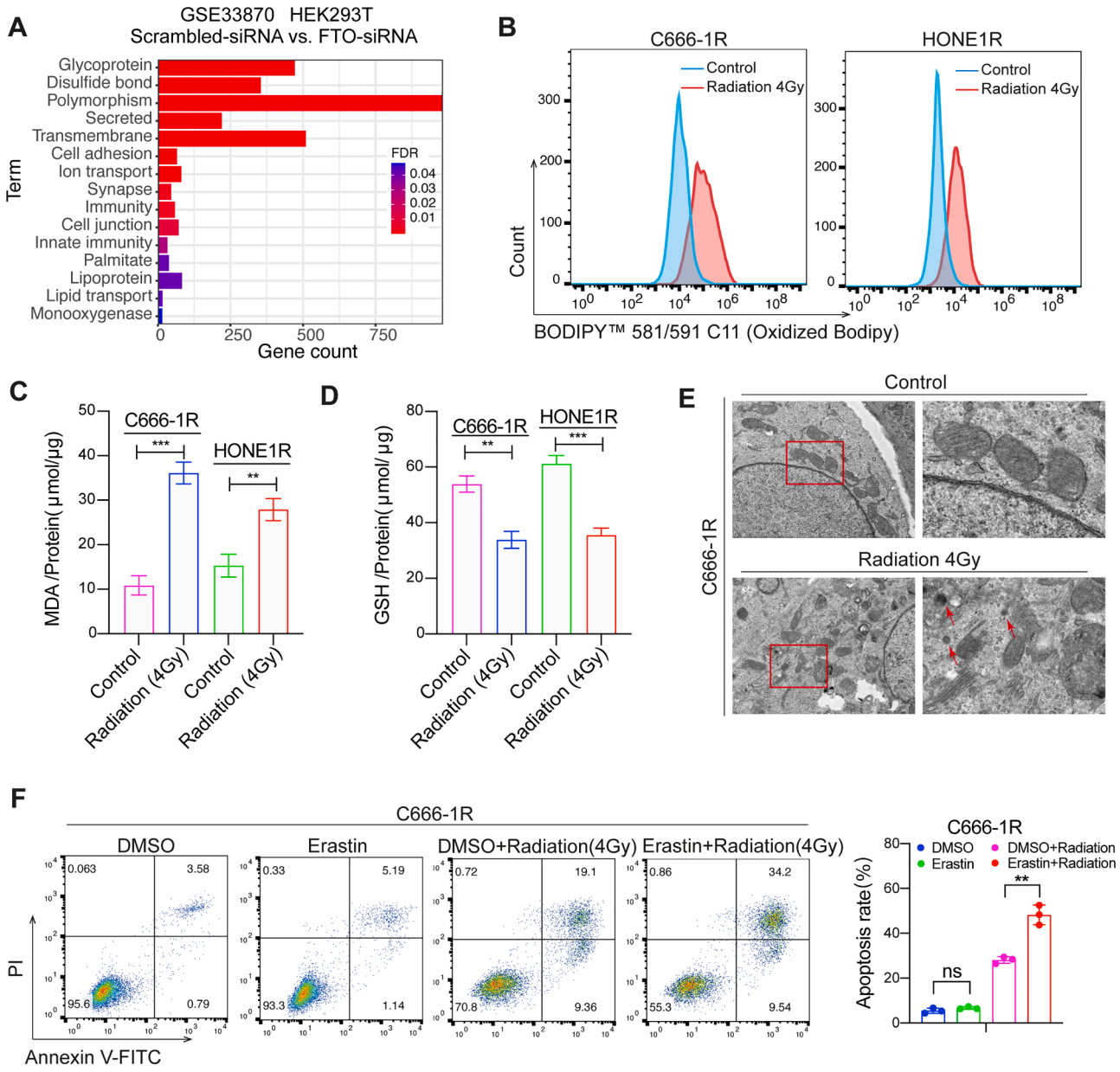

Fig. 4. Induction of ferroptosis contributes to the radiosensitivity of NPC cells. (A) Kyoto Encyclopedia of Genes and Genomes (KEGG) enrichment analysis showed that multiple deregulated genes were annotated in lipid metabolism pathways when knock down FTO in HEK293T cells. (B) Basal lipid peroxidation levels increased with cells exposure to radiation. Indicated cells were stained with C11-BODIPY 581/591. Reduced-BODIPY was measured by flow cytometry using a 488 nm laser and oxidized-BODIPY was measured with a 561 nm laser. A significant shift of oxidized-BODIPY occurred on exposure to radiation. (C) Cellular lipid peroxidation levels were measured by the malondialdehyde (MDA) kit. (D) Intracellular reduced glutathione (GSH) levels of NPC cells were significantly decreased with exposure to radiation. (E) Electron micrographs showing mitochondria in cells with or without radiation. (F) Cell apoptosis rate analyses of NPC cells that received the indicated treatments are shown.

modification of specific genes. Using the ENCORI (http://starbase.sysu.edu.cn/panCancer.php) database, we identified OTUB1 as a potential target of FTO. OTUB1 is a member of the ovarian tumor domain protease (OTU) subfamily of deubiquitinases (DUBs) and negatively regulates ubiquitination to control protein stability and activity [23]. Accumulating evidence has demonstrated that OTUB1 is a critical regulator of DNA damage response and cancer development [24]. In our recent study, we found that OTUB1 was upregulated in radiotherapy-resistant cells relative to radiotherapy-sensitive cells (Fig. 6B). In addition, we observed that the transcriptional and protein levels of OTUB1 increased with the high expression of FTO but decreased with the inhibition of FTO by FB23-2 in NPC cells (Fig. 6C).

Based on the Kaplan–Meier plotter database, we found that OTUB1 transcription was significantly correlated with poor survival in patients with HNSC (Fig. 6D). In addition, we found a positive correlation between OTUB1 and FTO transcription levels in HNSC (Fig. 6E), indicating the possibility of a regulatory relationship between FTO and OTUB1.

To confirm whether OTUB1 mRNA undergoes FTO-mediated m6A demethylation, we performed methylated RNA immunoprecipitation quantitative PCR, and the results revealed that the m6A abundance of OTUB1 mRNA was significantly decreased after FTO overexpression but increased following FTO enzyme activity inhibition (Fig. 6F). Similarly, the RIP-qPCR assay showed that OTUB1 mRNA was significantly enriched in the precipitates of FTO antibody, indicating the binding of OTUB1 transcripts to FTO protein (Fig. 6G).

A previous study demonstrated that OTUB1 mediates ferroptosis via

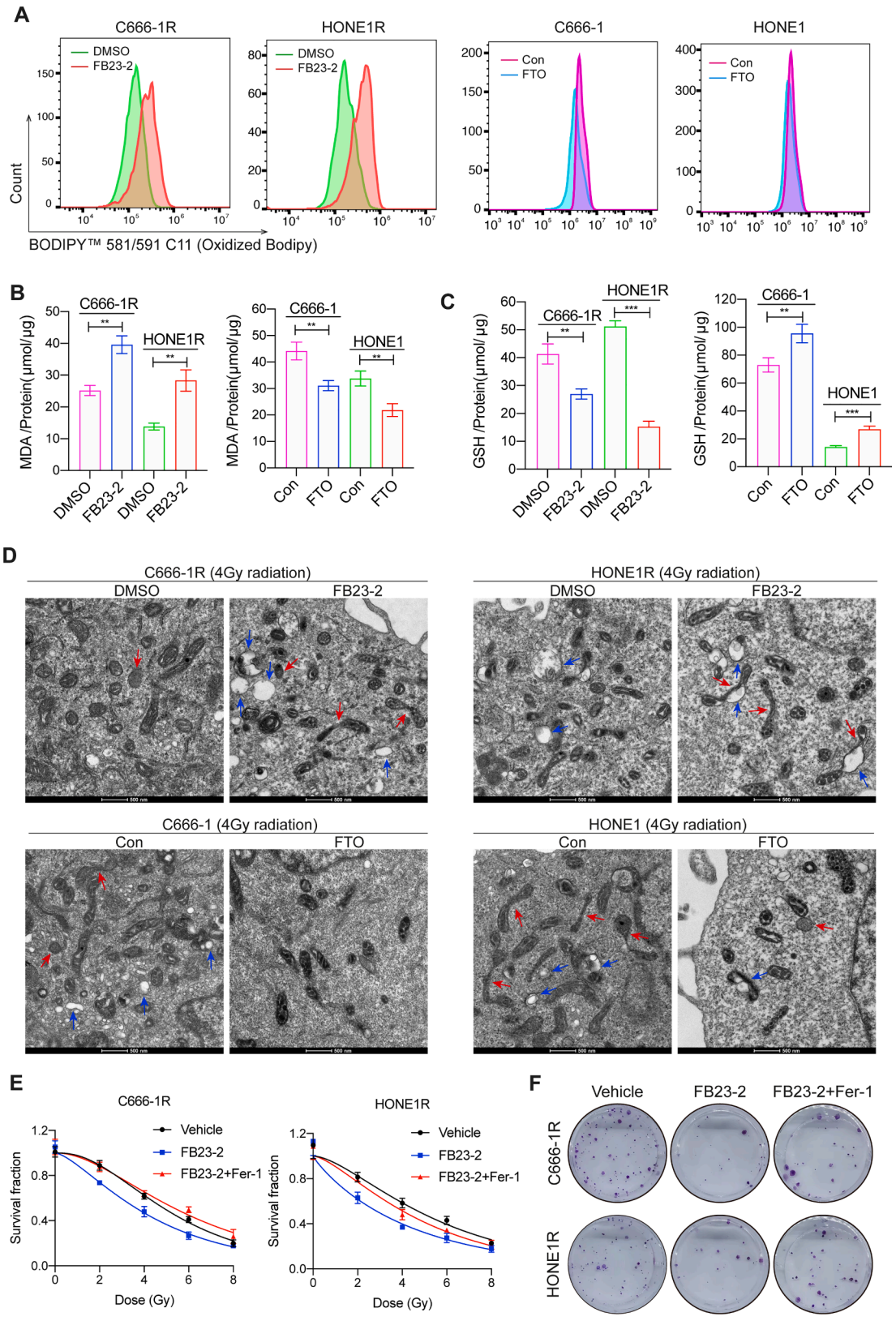

Fig. 5. FTO promotes radiotherapy resistance by antagonizing radiation-induced ferroptosis in NPC cells.
(A–C) BODIPY 581/591C11, MDA, and intracellular GSH were detected in NPC cells when treating cells with FB23-2 or overexpressed FTO combination with radiation (mean ± SEM, $n = 3$, two-sided t test). (D) Electron micrographs showing mitochondria in NPC cells treated with FB23-2 or overexpressed FTO, as well as corresponding control NPC cells. Red arrows showed the shrunken mitochondria. Blue arrows showed lipid droplets. (E) Dose responses of surviving factions of C666-1 and HONE1 cells that received the indicated treatments are shown. (F) Representative images of colony formation assay in NPC cells that received the indicated treatments are shown.

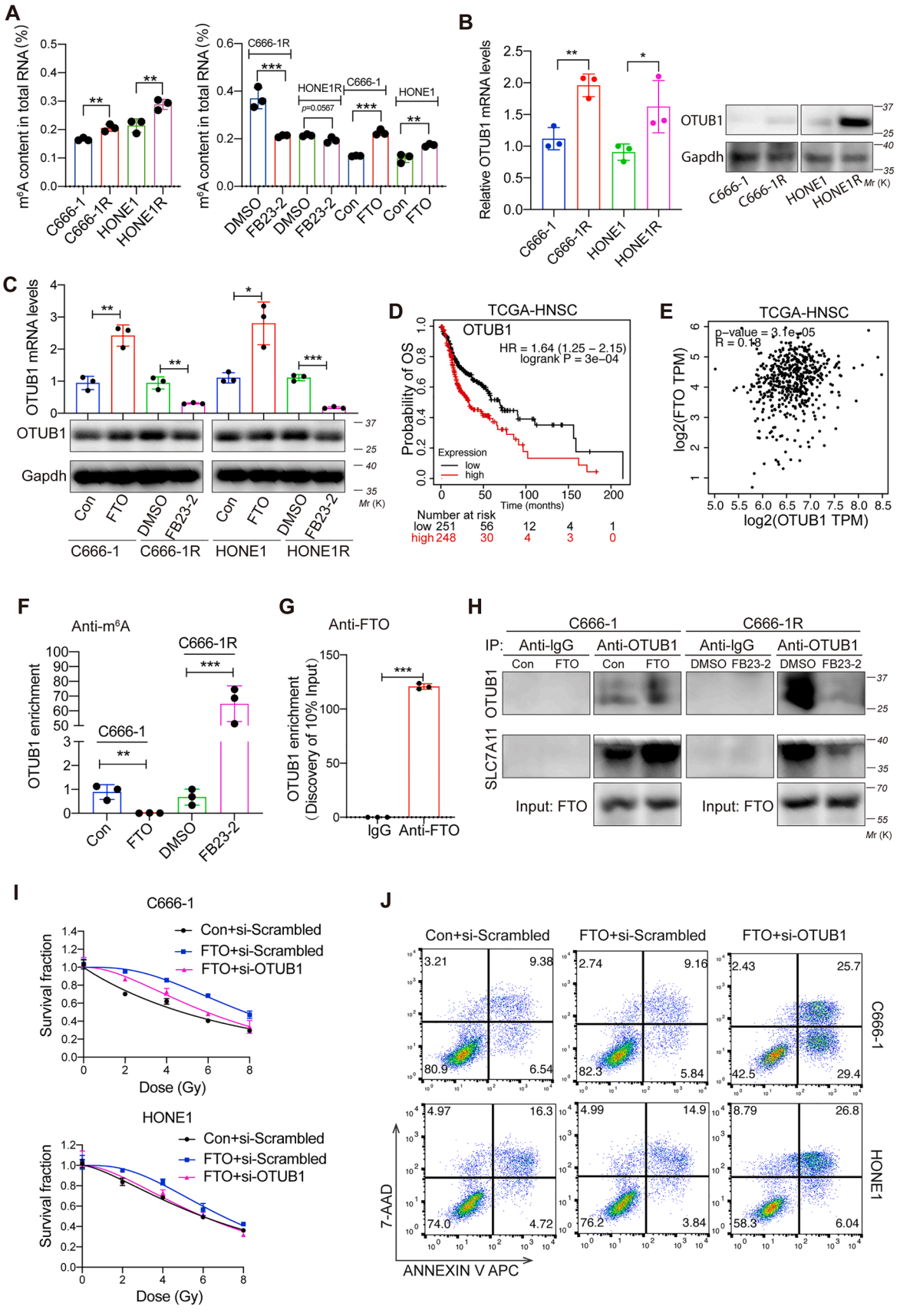

(caption on next page)

Fig. 6. FTO suppresses radiation-induced ferroptosis in an OTUB1 and SLC7A11-dependent manner.
(A) The m6A RNA methylation status in NPC cells were evaluated using an RNA Methylation Quantification Kit (mean ± SEM, $n = 3$, two-sided t test). (B) The transcription and protein levels of OTUB1 were evaluated by RT-qPCR and Western blot assay. (C) The transcription and protein levels of OTUB1 were detected when treating NPC cells with FB23-2 or overexpressing FTO. (D) Kaplan–Meier survival curves show the correlations between OTUB1 expression and overall survival (OS, p0.05) in patients with HNSC. (E) The transcription levels of OTUB1 were positively correlated with those of FTO in HNSC tissue samples. (F, G) RIP experiments were performed using antibodies against m6A and against FTO with extracts from NPC cells. (H) Western blot analysis of SLC7A11 and OTUB1 after immunoprecipitation of Anti-OTUB1 in NPC cells treated with FB23-2 or transfected with Flag-FTO; 2.5% of the sample was loaded as the input. (I) Dose responses of surviving factions of C666-1 and HONE1 cells that received the indicated treatments are shown. (J) Cell apoptosis of indicated NPC cells was quantified using Flow Cytometry assay.

the stabilization of SLC7A11 in human cancer [25]. Notably, our present study showed that FTO overexpression enhanced the interaction between SLC7A11 and OTUB1 in NPC cells (Fig. 6H). In addition, the rescue experiment showed that the downregulation of OTUB1 could partially reverse the radiotherapy resistance mediated by FTO overexpression (Fig. 6I, J).

Taken together, these results indicate that FTO upregulates the radioresistance of NPC cells by inhibiting ferroptosis by stabilizing the interaction between OTUB1 and SLC7A11.

Accelerating ferroptosis overcomes the radioresistance of NPC patient-derived xenografts

Finally, we sought to examine the effect of ferroptosis inducer erastin on tumor growth *in vivo* by using subcutaneous xenograft tumor models, including an NPC patient-derived xenograft model (NPC PDX). Our data revealed that the combination of erastin with radiation significantly inhibited the growth of xenograft tumors of HONE1R cells in nude mice compared to radiation alone ($P < 0.05$) (Fig. 7A, B). At the end of the experiment, the combination of erastin with radiation significantly decreased tumor volume and weight compared to radiation alone (Fig. 7C). We also utilized NPC PDX to further understand the effects of ferroptosis on NPC. As shown in Fig. 7D, recurrent tumor tissues in the nasopharynx of patients with NPC after radiotherapy were used to construct the PDX models. Histological comparison of the founder (P0) PDX tumors showed similarities with the corresponding patient tumor specimens (Fig. 7E). Consistently, erastin showed a significant radiosensitization effect in the PDX model (Fig. 7F). These results collectively support the notion that the combination of erastin and radiation is a promising strategy for NPC therapy.

Discussion

NPC is an EBV-related cancer that is especially prevalent in southern China, Southeast Asia, and North Africa [26]. Although the incidence of NPC has gradually declined in endemic regions, mortality due to this disease has fallen substantially over the past few decades [27]. However, 10–20% of patients diagnosed with NPC are radioresistant and ultimately experience recurrence and distant metastases [28]. Currently, the biomarkers and underlying mechanisms of radioresistance in NPC remain unclear. Therefore, the investigation of potential therapeutic targets for reversing radioresistance may represent a promising strategy for the treatment of NPC.

FTO belongs to the non-heme FeII/α-KG-dependent dioxygenase AlkB family of proteins and was recently identified as an m6A demethylase in vertebrates [29]. Several studies have demonstrated that FTO is strongly related to the onset and development of multiple tumors [13,19,30,31]. However, whether FTO affects the radiotherapy resistance of NPC remains unknown. In our recent study, we found that the transcription and translation levels of FTO increased in radiotherapy-resistant tissues and cells. Furthermore, a comprehensive database analysis showed that high FTO expression was predictive of poor survival and prognosis for patients with HNSC. Importantly, our *in vitro* and animal experiments showed that FTO promotes radiotherapy resistance in NPC. These findings sparked our interest in investigating the mechanism of FTO in radioresistance in NPC.

By analyzing the expression profile changes upon the knockdown of FTO expression in cells, we identified that some of the deregulated genes were involved in the regulation of lipoproteins, lipid transport, palmitate, and monooxygenase, all of which are hallmarks of ferroptosis. Previous studies have shown that radiotherapy directly induces ferroptosis by upregulating critical regulators of ferroptosis, including SLC7A11 and ACSL4, in cancer cells [32]. Thus, we explored the regulatory relationship between FTO and ferroptosis in NPC radioresistance. Not surprisingly, in our recent study, we observed that radiation led to an increase in cellular lipid peroxidation in NPC, which ultimately resulted in ferroptosis. Furthermore, we identified radioresistant NPCs to be exquisitely radiation-sensitive when combined with the ferroptosis inducer erastin. Moreover, our further studies showed that forced expression of FTO enhanced lipid peroxidation accumulation and triggered mitochondrial shrinkage in NPC cells, while inhibition of FTO activity by FB23-2 induced the opposite result. We found that the use of a ferroptosis inhibitor (Fer-1) can reverse the radiation sensitivity of NPC cells induced by the FTO inhibitor FB23-2. Thus, the function of FTO in inducing ferroptosis likely plays a critical role in NPC radioresistance.

Several studies have demonstrated that FTO is an N6-methyladenosine (m6A) demethylase in eukaryotic cells [33]. On analyzing data from the ENCORI database, we identified OTUB1, a deubiquitinase that stabilizes the ferroptosis inhibitor SLC7A11 and eventually promotes tumorigenesis in human cancers [25], as a potential downstream molecule regulated by FTO. Additionally, analysis of data obtained from the GEPIA database revealed a significantly positive correlation between OTUB1 and FTO expressions, and a high level of OTUB1 was predictive of poor prognosis in the HNSC dataset. In the current study, although FTO increases the abundance of m6A in transcriptomes, which may be due to the involvement of FTO in the regulation of methylase proteins, FTO can reduce the level of m6A modification of OTUB1 mRNA and promote the expression of OTUB1 in NPC cells. Furthermore, the downregulation of OTUB1 could reverse FTO-induced RT resistance to an extent *in vitro*, which further corroborated that FTO may attenuate radiation-triggered ferroptosis by stabilizing OTUB1 and SLC7A11 in NPC.

Erastin has been identified as a ferroptosis activator that selectively triggers cancer cell death by targeting SLC7A11 [22]. Accumulating evidence confirmed that erastin has a robust effect on the suppression of tumor survival *in vitro* and in mice tumor models [22,33]. Based on the finding that erastin sensitized NPC cells to radiation *in vitro*, we further examined the effect of erastin on tumor growth *in vivo* using subcutaneous xenograft tumor models, including a radioresistant PDX model established by radiotherapy-resistant NPC tissues. Our data revealed that the combination of erastin and radiotherapy effectively inhibited the growth of xenograft tumors in mice compared to radiotherapy alone.

Although our research showed some novel findings, there are several limitations in our present research. First, we did not verify the effect of FTO on the radiosensitivity of NPC cells by knocking down FTO expression *in vitro* or *in vivo*. Further studies that silence FTO expression by siRNA or shRNA are necessary to further explore the effect of FTO on the therapeutic response of NPC. Second, we did not use clinical specimens of NPC to confirm the correlation between FTO expression and prognosis of patients with NPC. Third, we used RNA-seq data in 293T rather than NPC cell line for enrichment analysis, which is a limitation of

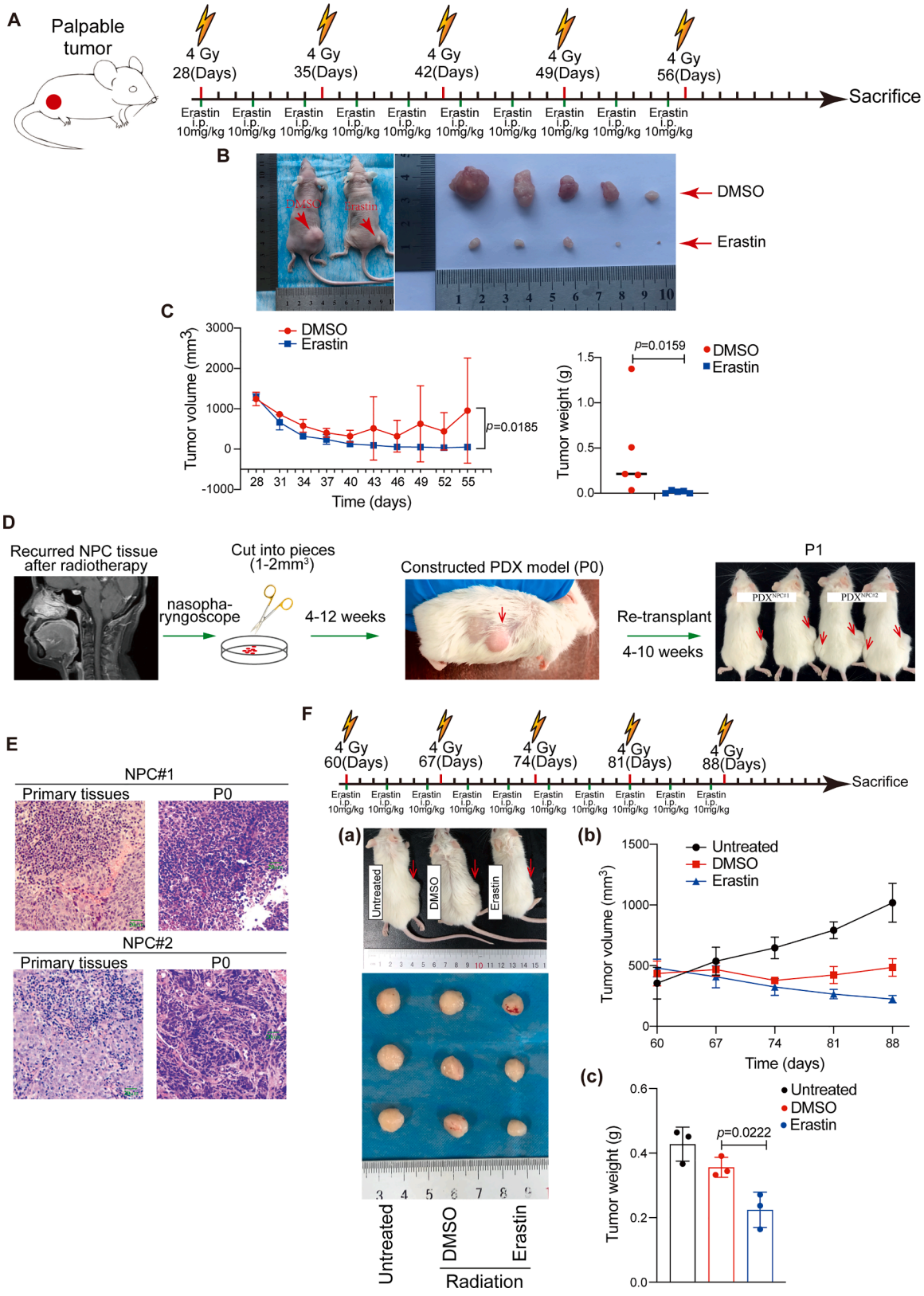

Fig. 7. Accelerating ferroptosis overcomes radioresistance of NPC patient-derived xenografts. (A) Outline of the experimental approach. (B) Images of subcutaneous tumors comprising HONE1R cells after treating with erastin or DMSO (vehicle) ($n = 5$). (C) (Left) The growth curves of subcutaneous tumors derived from HONE1R cells with or without erastin in combination with radiotherapy are shown; (Right) Tumor weight was measured at the endpoint. (D) Outline of the experimental approach, beginning with the primary sample. (E) Histological comparison of the founder (P0) PDX tumor and primary patient-derived specimens. (F) (a) Images of tumor-bearing mice and subcutaneous tumors derived from mice; (b) the growth curves of xenografted tumor derived from mice treated with erastin or DMSO (vehicle) and under 20 Gy radiotherapy; (c) tumor weight was measured at the endpoint (mean ± SEM, two-sided t test).

our study, because the m6A modification is dynamic and context dependent. Finally, we have not confirmed the mechanism of FTO-mediated radiotherapy resistance of NPC in animal models. Future studies should investigate the detailed functions and mechanisms of FTO in NPC.

In conclusion, the findings reported in this paper highlight the protective effects of FTO against ferroptotic cell death by erasing the m6A modification of OUTB1 transcripts and enhancing the expression of OUTB1 in NPC. FTO may be used as a novel biomarker for the diagnosis and prognosis of NPC after radiotherapy. Additionally, it will be of great benefit to expand the research on FTO in NPC as a potential therapeutic target for radiosensitization in the future.

Ethics approval and consent to participate

Fresh NPC tissues were obtained from the First Affiliated Hospital of Guangxi Medical University and approved by the appropriate ethics committee. Research involving animals was performed in compliance with the policies of the animal ethics committee of the Guangxi Medical University of China (Nanning, China; NO: 2021-KY-National Natural Science-091).

Consent for publication

All authors approved to publish the study in this journal.

Availability of data and materials

All data created or analyzed during this study are enrolled in this published article or are available from the corresponding author on reasonable request.

CRediT authorship contribution statement

Wei-Mei Huang: Conceptualization, Data curation, Investigation, Writing – original draft. **Zhi-Xun Li:** Methodology, Resources, Writing – review & editing. **Ying-Hui Wu:** Conceptualization, Methodology, Writing – review & editing. **Zhi-Ling Shi:** Data curation, Methodology. **Jing-Lin Mi:** Validation, Visualization. **Kai Hu:** Supervision. **Ren-Sheng Wang:** Supervision, Funding acquisition.

Declaration of Competing Interest

The authors declare that they have no competing interests.

Acknowledgments

Not applicable.

Funding

This work was supported by the National Natural Science Foundation of China (Nos. 5 81360405).

Supplementary materials

Supplementary material associated with this article can be found, in the online version, at doi:10.1016/j.tranon.2022.101576.

References

[1] K. Wong, et al., Nasopharyngeal carcinoma: an evolving paradigm, Nat. Rev. Clin. Oncol. 18 (11) (2021) 679–695.
[2] D. Ou, et al., Induction chemotherapy with docetaxel, cisplatin and fluorouracil followed by concurrent chemoradiotherapy or chemoradiotherapy alone in locally advanced non-endemic nasopharyngeal carcinoma, Oral Oncol. 62 (2016) 114–121.
[3] P. Bossi, et al., Nasopharyngeal carcinoma: ESMO-EURACAN clinical practice guidelines for diagnosis, treatment and follow-up, Ann. Oncol. 32 (4) (2021) 452–465, official journal of the European Society for Medical Oncology.
[4] K. Au, et al., Treatment outcomes of nasopharyngeal carcinoma in modern era after intensity modulated radiotherapy (IMRT) in Hong Kong: A report of 3328 patients (HKNPCSG 1301 study), Oral Oncol. 77 (2018) 16–21.
[5] S. Moon, et al., IMRT vs. 2D-radiotherapy or 3D-conformal radiotherapy of nasopharyngeal carcinoma: Survival outcome in a Korean multi-institutional retrospective study (KROG 11-06), Strahlenther. Onkol. 192 (6) (2016) 377–385.
[6] A. Lee, et al., Management of locally recurrent nasopharyngeal carcinoma, Cancer Treat. Rev. 79 (2019), 101890.
[7] S. Garbo, et al., m6A RNA methylation and beyond - the epigenetic machinery and potential treatment options, Drug Discov. Today 26 (11) (2021) 2559–2574.
[8] M. Uddin, et al., The mA RNA methylation regulates oncogenic signaling pathways driving cell malignant transformation and carcinogenesis, Mol. Cancer 20 (1) (2021) 61.
[9] O. Shriwas, et al., The impact of m6A RNA modification in therapy resistance of cancer: implication in chemotherapy, radiotherapy, and immunotherapy, Front. Oncol. 10 (2020), 612337.
[10] B. Chen, et al., Development of cell-active N6-methyladenosine RNA demethylase FTO inhibitor, J. Am. Chem. Soc. 134 (43) (2012) 17963–17971.
[11] R. Su, et al., Targeting FTO suppresses cancer stem cell maintenance and immune evasion, Cancer Cell 38 (1) (2020) 79–96.e11.
[12] S. Relier, et al., FTO-mediated cytoplasmic mA demethylation adjusts stem-like properties in colorectal cancer cell, Nat. Commun. 12 (1) (2021) 1716.
[13] Y. Niu, et al., RNA N6-methyladenosine demethylase FTO promotes breast tumor progression through inhibiting BNIP3, Mol. Cancer 18 (1) (2019) 46.
[14] X. Chen, et al., Broadening horizons: the role of ferroptosis in cancer, Nat. Rev. Clin. Oncol. 18 (5) (2021) 280–296.
[15] G. Lei, et al., Ferroptosis as a mechanism to mediate p53 function in tumor radiosensitivity, Oncogene 40 (20) (2021) 3533–3547.
[16] Y. Huang, et al., Small-molecule targeting of oncogenic FTO demethylase in acute myeloid leukemia, Cancer Cell 35 (4) (2019) 677–691.e610.
[17] S. Alvarez, et al., NFS1 undergoes positive selection in lung tumours and protects cells from ferroptosis, Nature 551 (7682) (2017) 639–643.
[18] W. Huang, et al., Circular RNA cESRP1 sensitises small cell lung cancer cells to chemotherapy by sponging miR-93-5p to inhibit TGF-β signalling, Cell Death Differ. 27 (5) (2020) 1709–1727.
[19] D. Wang, et al., N-methyladenosine RNA demethylase FTO promotes gastric cancer metastasis by down-regulating the m6A methylation of ITGB1, Front. Oncol. 11 (2021), 681280.
[20] H. Wei, et al., The role of FTO in tumors and it's research progress, Curr. Med. Chem. 29 (5) (2022) 924–933.
[21] T. Berulava, et al., FTO levels affect RNA modification and the transcriptome, Eur. J. Hum. Genet. EJHG 21 (3) (2013) 317–323.
[22] X. Chen, et al., Broadening horizons: the role of ferroptosis in cancer, Nat. Rev. Clin. Oncol. 18 (5) (2021) 280–296.
[23] M. He, et al., Emerging role of DUBs in tumor metastasis and apoptosis: therapeutic implication, Pharmacol. Therapeutics 177 (2017) 96–107.
[24] M. Saldana, et al., Otubain 1: a non-canonical deubiquitinase with an emerging role in cancer, Endocr. Relat. Cancer 26 (1) (2019) R1–R14.
[25] T. Liu, et al., The deubiquitylase OTUB1 mediates ferroptosis via stabilization of SLC7A11, Cancer Res. 79 (8) (2019) 1913–1924.
[26] Y. Chen, et al., Nasopharyngeal carcinoma, Lancet 394 (10192) (2019) 64–80 (London, England).
[27] M. Chua, et al., Nasopharyngeal carcinoma, Lancet 387 (10022) (2016) 1012–1024 (London, England).
[28] V. Lee, et al., Palliative systemic therapy for recurrent or metastatic nasopharyngeal carcinoma - how far have we achieved? Crit. Rev. Oncol. Hematol. 114 (2017) 13–23.
[29] G. Jia, et al., N6-methyladenosine in nuclear RNA is a major substrate of the obesity-associated FTO, Nat. Chem. Biol. 7 (12) (2011) 885–887.
[30] Z. Li, et al., FTO plays an oncogenic role in acute myeloid leukemia as a N-methyladenosine RNA demethylase, Cancer Cell 31 (1) (2017) 127–141.
[31] J. Chen, et al., Novel positioning from obesity to cancer: FTO, an mA RNA demethylase, regulates tumour progression, J. Cancer Res. Clin. Oncol. 145 (1) (2019) 19–29.
[32] A. Pearson, et al., Contribution of lipid oxidation and ferroptosis to radiotherapy efficacy, Int. J. Mol. Sci. 22 (22) (2021) 377–385.
[33] J. Cai, et al., Natural product triptolide induces GSDME-mediated pyroptosis in head and neck cancer through suppressing mitochondrial hexokinase-II, J. Exp. Clin. Cancer Res. CR 40 (1) (2021) 190.